Cancer Research

Photodynamic Therapy Synergizes with Irinotecan to Overcome Compensatory Mechanisms and Improve Treatment Outcomes in Pancreatic Cancer

Huang-Chiao Huang[1,2], Srivalleesha Mallidi[1,2], Joyce Liu[1,2], Chun-Te Chiang[1,2], Zhiming Mai[1,2], Ruth Goldschmidt[1,2], Neema Ebrahim-Zadeh[1,2], Imran Rizvi[1,2], and Tayyaba Hasan[1,2,3]

Abstract

The ability of tumor cells to adapt to therapeutic regimens by activating alternative survival and growth pathways remains a major challenge in cancer therapy. Therefore, the most effective treatments will involve interactive strategies that target multiple nonoverlapping pathways while eliciting synergistic outcomes and minimizing systemic toxicities. Nanoliposomal irinotecan is approved by the FDA for gemcitabine-refractory metastatic pancreatic cancer . However, the full potential of irinotecan treatment is hindered by several cancer cell survival mechanisms, including ATP-binding cassette G2 (ABCG2) transporter-mediated irinotecan efflux from cells. Here, we demonstrate that benzoporphyrin derivative-based photodynamic therapy (PDT), a photochemical cytotoxic modality that activates the apoptotic pathway, reduced ABCG2 expression to increase intracellular irinotecan levels in pancreatic cancer. Moreover, we show that PDT inhibited survivin expression. Although PDT potentiated irinotecan treatment, we also demonstrate that irinotecan reduced the tumoral expression of monocarboxylate transporter 4, which was upregulated by PDT. Notably, using orthotopic xenograft models, we demonstrate that combination of single low-dose PDT and a subclinical dose of nanoliposomal irinotecan synergistically inhibited tumor growth by 70% for 3 weeks compared with 25% reduction after either monotherapies. Our findings offer new opportunities for the clinical translation of PDT and irinotecan combination therapy for effective pancreatic cancer treatment. *Cancer Res; 76(5); 1066–77. ©2015 AACR.*

Introduction

Cancer cells can ingeniously adapt themselves to therapeutic insults by adjusting their growth and survival signaling circuitry through cross-talk loops (1). Thus, there is an increasing focus on combination therapies that offer enhanced effects by imparting damage to different cellular compartments and molecular pathways (2). Besides their therapeutic benefits, these combinations are more attractive and viable for translation if the agents are approved by the FDA and have nonoverlapping side effects (2).

Irinotecan, a camptothecin derivative, is approved for treatment of pancreatic and other cancers. This S-phase–specific chemotherapeutic agent inhibits topoisomerase I action by binding to topoisomerase–DNA complexes, preventing DNA religation, causing DNA-strand breaks, and leading to cell death (3). In a recent phase III trial for patients with gemcitabine-refractory metastatic pancreatic cancer, a nanoliposomal irinotecan formulation (MM-398) combined with fluorouracil and leucovorin extended the median overall survival (OS, primary endpoint) to 6.1 months, compared with 4.2 months for the fluorouracil and leucovorin control (4, 5). This marginal improvement in OS was viewed as a significant breakthrough, highlighting the dismal nature of pancreatic cancer, and reaffirming the need for alternative, intelligently designed interventions.

Although efforts have been made to develop chemotherapeutic and biologic cocktails to address challenges, such as multidrug resistance and upregulation of survival pathways, these attempts have largely been hindered by high toxicities associated with these agents adding to the already toxic regimens. It is, therefore, important to devise combinations that complement each other mechanistically to abrogate resistance pathways, while minimizing systemic toxicities.

Photodynamic therapy (PDT) is a well-established photochemistry-based approach where a noncytotoxic agent (i.e., photosensitizer) is excited by appropriate wavelength light to generate cytotoxic molecular species, killing or modulating cells (6). PDT uniquely stimulates cell death by directly activating apoptosis, and therefore bypasses many cell death signaling pathways required for chemoradiation to be effective. Kessel and colleagues first report that PDT-induced mitochondrial photodamage results

[1]Wellman Center for Photomedicine, Massachusetts General Hospital (MGH) and Harvard Medical School, Boston, Massachusetts. [2]Department of Dermatology, MGH, Boston, Massachusetts. [3]Division of Health Sciences and Technology, Harvard University and Massachusetts Institute of Technology, Cambridge, Massachusetts.

Note: Supplementary data for this article are available at Cancer Research Online (http://cancerres.aacrjournals.org/).

H.-C. Huang and S. Mallidi contributed equally to this article.

Corresponding Author: Tayyaba Hasan, Harvard Medical School, Massachusetts General Hospital, 40 Blossom Street, BAR 314A, Boston, MA 02114. Phone: 617-726-6996; Fax: 617-724-1345; E-mail: thasan@mgh.harvard.edu

doi: 10.1158/0008-5472.CAN-15-0391

in loss of mitochondrial membrane potential, destruction of mitochondria-associated Bcl-2, release of cytochrome *c* and subsequent apoptosis initiation (7), a finding confirmed by Xue and colleagues (8). This direct induction of apoptosis makes PDT effective even against chemo/radio-resistant cancers with defective signaling pathways (9). Several studies have also shown that the unique mechanisms of cell death activated by PDT can resensitize drug-resistant cells (10) and synergize with both chemo and biologic therapies, such as receptor tyrosine kinase inhibitors (11, 12). Gallagher-Colombo and colleagues showed that priming PDT with EGFR inhibitor erlotinib improved treatment efficacy in non–small cell lung carcinoma xenografts, even in erlotinib-resistant tumors (11). Our group has demonstrated that PDT cooperates mechanistically with anti-EGFR antibody, Erbitux, to synergistically increase survival in disseminated ovarian cancer models (12). In the context of chemotherapeutic combinations, Duska and colleagues showed that PDT via photoimmunoconjugates enhanced the cytotoxicity of cisplatin in ovarian cancer, and such enhancement is also synergistic on platinum-resistant cells (10). PDT, which has received regulatory approval worldwide, is already a successful adjuvant therapy in clinical trials for several malignancies where most therapies have failed. For pancreatic cancer, Bown and colleagues showed that chlorin-based PDT improved the median survival from 6–10 to 12.5 months in locally advanced pancreatic cancer patients (13). Our phase I/II trial reaffirms that benzoporphyrin derivative (BPD)-based PDT consistently induced tumor necrosis at 40 J/cm in patients with localized pancreatic cancer (14).

Here, we demonstrate multiple cooperative mechanistic interactions between PDT and irinotecan, showing for the first time that PDT reduces ATP-binding cassette G2 (ABCG2) efflux transporter expression to increase intracellular irinotecan concentrations and that PDT inhibits survivin expression to enhance apoptosis. We also show that irinotecan reduces the tumoral expression of the monocarboxylate transporter 4 (MCT-4), a biomarker that was upregulated by PDT. The combination of PDT and irinotecan is also attractive for cancer treatment due to their nonoverlapping side effects. The systemic toxicities associated with irinotecan include grade 3–4 diarrhea and neutropenia (4), and patients often require dose reduction or preemptive management. In contrast, PDT is well tolerated in pancreatic cancer treatment and the only major adverse event of "mild" abdominal pain can be alleviated using analgesics (14). Therefore, we hypothesize that a low-dose PDT and irinotecan combination (12- to 20-fold lower than equivalent clinical effective doses; Supplementary Table S1) would be more tolerable and synergistic due to the unique counterbalancing mechanisms.

Advances in nanoliposomes have provided the means to preferentially deliver chemotherapeutic agents or photosensitizers to tumors, reducing systemic toxicities and improving outcomes (15). Clinically, nanoliposomes improved the pharmacokinetics and biodistribution of irinotecan, minimizing side effects (4). Non-pegylated nanoliposomal BPD (Visudyne) is approved by the FDA for the treatment of age-related macular degeneration, and used in pancreatic cancer clinical studies (14). Encouraged by these clinical advances, and motivated by the need for innovative, easily translatable treatments, we hypothesized that the distinct mechanisms of PDT and irinotecan, combined with mutually reinforcing molecular responses, would provide synergistic outcomes. Using nanoliposomal formulations of BPD and irinotecan, we investigated the antitumor efficacy of low-dose combination therapy in orthotopic MIA PaCa-2 and AsPC-1 tumor models.

Materials and Methods

Nanoliposome preparation and characterization

Nanoliposomal BPD (L-BPD) and nanoliposomal irinotecan (L-IRI) were prepared via freeze–thaw extrusion (Supplementary Methods; ref. 15). Zetasizer NanoZS (Malvern) measured particle size and zeta potential. Concentrations of BPD and irinotecan were determined based on their absorbance spectra in DMSO using established molar extinction coefficients (BPD: $\varepsilon = 34{,}895$ $M^{-1}cm^{-1}$ at 687 nm; Irinotecan: $\varepsilon = 21{,}835$ $M^{-1}cm^{-1}$ at 384 nm). Entrapment efficacy is defined as the molar ratio of drug entrapped into nanoliposomes to total drug added initially. Loading capacity is determined on the basis of the ratio of final drug weight to overall weight of the nanoliposomes. BPD quenching, photobleaching, and singlet oxygen ($^1O_2$) generation were studied in 96-well plates. L-BPD and singlet oxygen sensor green (SOSG) at 5 μmol/L were irradiated with 690-nm light at different fluences (0–75 J/cm^2, 50 mW/cm^2, Intense-High Power Devices, Series-7401). A microplate reader (Molecular Devices) acquired fluorescence signals of BPD (Ex/Em:422/650–750 nm) or SOSG (Ex/Em:504/525 nm) before and after irradiation. Drug release was studied in 10% human serum at 37°C using dialysis.

In vitro molecular characterization post-PDT

MIA PaCa-2 and AsPC-1 cells were obtained from ATCC between 2012 and 2015, cultured as per manufacturer's instructions, and tested for mycoplasma contamination. A total of 150,000 cells grown overnight were incubated with L-BPD (250 nmol/L) for 1 hour. Before PDT, L-BPD–containing medium was replaced with fresh medium. Cells were irradiated with 690-nm light at different fluences (0.5–5 J/cm^2, 50 mW/cm^2). At 1, 6, or 24 hours post-PDT, detached cells were removed via phosphate buffered saline (PBS) washes and remaining cells assessed for viability (MTT assay, Invitrogen) or biomarkers (ABCG2, survivin) by immunofluorescence and immunoblotting (Supplementary Methods).

Evaluation of intracellular irinotecan accumulation post-PDT

A total of 250,000 cells grown overnight were incubated in medium containing L-BPD (250 nmol/L) and L-IRI (0.24 mg/mL) for 1 hour. Before PDT (690 nm, 0.5 J/cm^2), the medium was replaced with either L-IRI–containing medium or "drug-free" medium. At 1 or 6 hours post-PDT, cells were washed and lysed with Solvable. A microplate reader (Molecular Devices) measured fluorescence signal from irinotecan (Ex/Em:355/460 nm) and its metabolite SN-38 (Ex/Em:355/538 nm). Readouts were normalized to protein concentration (Pierce BCA Protein Assay).

Orthotopic mouse model

Animal protocols were approved by MGH Institutional Animal Care and Use Committee (IACUC). Orthotopic MIA PaCa-2 or AsPC-1 tumors were established in male athymic (nu/nu) Swiss mice (4–6 weeks old). A 1-cm incision on the left abdominal flank was made to exteriorize the pancreas of ketamine/xylazine–anesthetized mouse. Cancer cells (1×10^6) suspended in 50 μL

medium-Matrigel mixture, were injected into the pancreas, and the incision was sutured aseptically.

Pharmacokinetics and biodistribution of L-BPD and L-IRI

Tumor-bearing mice received intravenous injection of L-IRI (20 mg/kg) and L-BPD (0.25 mg/kg). Blood, tumor, and tissues were collected 10 minutes, 1, 4, 12, and 24 hours postinjections. BPD and irinotecan were extracted from tissue samples (Supplementary Methods), and then quantified via liquid chromatography/tandem mass spectrometry (LC/MS-MS, Agilent) for the determination of %ID/g (percentage injected dose per gram tissue).

In vivo combination treatment

Treatments were initiated 9 days postimplantation when tumors reached approximately 25 mm^3 (Supplementary Fig. S1A). One hour post-intravenous injection of low-dose L-BPD (0.25 mg/kg) and L-IRI (20 mg/kg), an incision was made on the left abdominal flank to exteriorize the tumor of anesthetized mice. A vertical light beam was focused on the tumor, and cloth was used to protect animal skin from light exposure. PDT was performed with a 690-nm laser (75 J/cm^2, 100 mW/cm^2). Light irradiation coincides with the BPD Q-band absorbance (Fig. 1A, arrow) without overlapping with irinotecan absorbance. Posttreatment, incisions were sutured. Tumor growth in every animal was longitudinally monitored every 3 to 5 days using noninvasive ultrasound imaging (Supplementary Methods). At each time point, tumor volume was calculated using ellipsoid estimation (width $\times$ length $\times$ height $\times \pi/6$), which was validated against the three-dimensional volume reconstruction algorithm of the Vevo2100 software (Supplementary Fig. S1B and S1C). Animals were euthanized on day 30. Collected tissues were processed for (i) histologic (hematoxylin and eosin stain, H&E) analysis of necrosis and (ii) immunofluorescence analysis of microvessel density (MVD, CD31 vascular endothelial marker) and proliferation (Ki-67; Supplementary Methods). In a small group of animals, tumors were excised at 24 hours posttreatment to analyze hypoxia (pimonidazole) and biomarker (MCT-4; Supplementary Methods and Table S2). H&E and immunofluorescence slides were imaged using a whole slide scanning fluorescence imaging system (Hamamatsu) or a confocal microscope (Olympus; Supplementary Methods). In a separate study, mice were treated with two cycles of combination therapy on days 9 and 27 postimplantation.

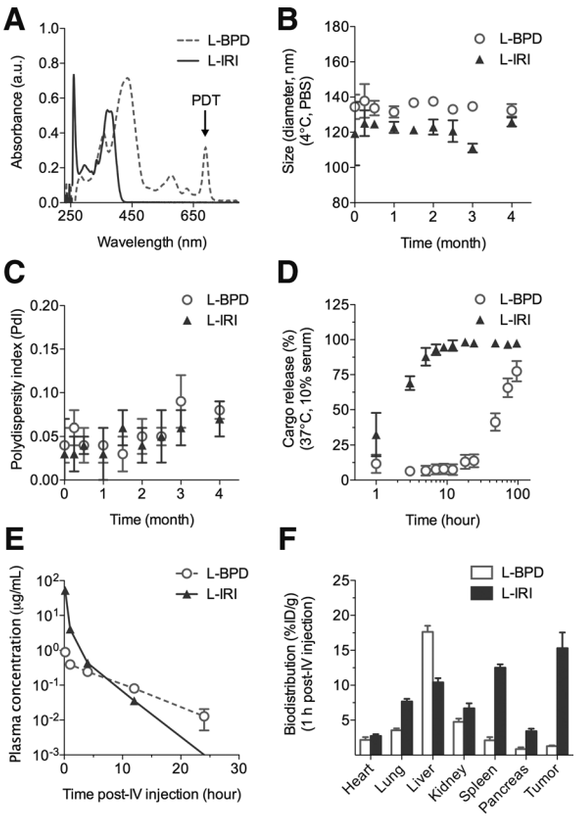

Figure 1.
Physical characterization of L-BPD (red) and L-IRI (blue). A, absorption spectra of L-BPD and L-IRI in DMSO. Arrow, light excitation wavelength. B and C, long-term stability of L-BPD and L-IRI stored in dark conditions (4°C) determined by size and polydispersity. D, L-BPD and L-IRI exhibit differential drug release profiles under biologically relevant conditions (37°C, 10% serum). E, plasma pharmacokinetics of L-BPD (0.25 mg/kg) and L-IRI (20 mg/kg) in athymic nu/nu mice. F, tissue biodistribution of L-BPD (0.25 mg/kg) and L-IRI (20 mg/kg) in tumor-bearing mice at 1-hour post-intravenous injection. Extracts from tissue homogenates were analyzed by LC/MS-MS ($N \geq 3$). IV, intravenous.

Statistical analysis

To compare treatment responses, one-way ANOVA statistical tests were carried out to avoid type-I error (GraphPad Prism). Synergy between PDT and L-IRI is determined to be significant via random slopes model (Supplementary Methods and Supplementary Table S3). Results are presented in mean $\pm$ SEM.

Results

Synthesis and characterization of nanoliposomes

For L-BPD and L-IRI syntheses, lipid compositions of dipalmitoylphosphatidylcholine, cholesterol, and distearoylphosphatidylethanolamine-methoxy polyethylene glycol were used on the basis of clinically approved formulations (15). Both L-BPD and L-IRI were grafted with 3 mol% of polyethylene glycol and are approximately 120 to 135 nm with a narrow size distribution (polydispersity index, $PdI < 0.1$; Supplementary Table S4). The surface charge of nanoliposomes was engineered to be neutral-to-slightly cationic (+12 mV), by introducing dioleoyltrimethylammoniumpropane (8 mol%) to the lipid composition, to balance toxicity, circulation, and tumor accumulation (15). Concentrations of BPD or irinotecan in nanoliposomes were determined on the basis of their respective absorbance spectra in DMSO (Fig. 1A). BPD was loaded in the lipid-bilayer via hydrophobic and ionic interactions (16) at entrapment efficiency of 70.7 $\pm$ 8%. Hydrophilic irinotecan was encapsulated in the aqueous core through passive equilibration (17) at a lower entrapment efficiency of 56.6 $\pm$ 4%. L-IRI loading capacity (10.2 $\pm$ 1%) was higher than that of L-BPD (0.42 $\pm$ 0.05%) due to the high aqueous-to-lipid compartment volume ratio of nanoliposomes (18). This corresponded to approximately 14,000 irinotecan molecules per L-IRI, and 600 BPD molecules per L-BPD. Our long-term stability study suggested that 4-month dark storage at 4°C did not affect overall size or monodispersity of nanoliposomes (Fig. 1B and C).

Drug release profiles of L-BPD and L-IRI were evaluated under biologically relevant conditions (37°C, 10% serum). At 1 hour postincubation, approximately 10% and 30% of BPD and irinotecan were released from nanoliposomes, respectively (Fig. 1D). Relatively fast drug release from L-IRI ($t_{1/2} = 2$ hours) compared with L-BPD ($t_{1/2} = 48$ hours) suggests that irinotecan will be readily available to tumors when PDT is in action.

Our *in vivo* pharmacokinetic study (Fig. 1E) shows that plasma clearance of L-IRI (clearance rate, pCL: 0.61L/kg × hour; AUC: 32.52 μg × hour/mL) is faster than that of L-BPD (pCL: 0.06 L/kg × hour; AUC: 4.267 μg × hour/mL). It is important to note that plasma clearance of L-IRI is still significantly slower than that of free irinotecan (pCL: 2.61 L/kg × hour; AUC: 7.65 μg × hour/mL; ref. 19). This suggests that nanoliposomes improve the circulation profile of irinotecan, an important factor in the cytotoxicity of irinotecan. At 1 hour post-intravenous injection, accumulation of irinotecan was higher in tumor (15.3 ± 2.2%ID/g) than in normal pancreas (3.4 ± 0.3%ID/g). Liver and spleen were organs of major L-BPD and L-IRI accumulation, respectively (Fig. 1F).

Photostability and photoactivity of L-BPD

Nanoliposomes have been shown to maintain the stability and photoactivity of photosensitizers in biologically relevant environments for effective PDT (20). However, photosensitizers could also be prone to self-quenching when packed in lipid bilayers at high concentrations (16). Here, we evaluated the photostability and quenching of free BPD and L-BPD by monitoring changes in BPD absorbance and fluorescence before and after dissolution in different solvents. In our BPD stability studies, the absorbance value at 690 nm for free BPD in PBS was reduced by 81.3 ± 3% compared with free BPD fully dissolved in DMSO, indicating a rapid aggregation of free BPD molecules in PBS (Fig. 2A). Aggregation of free BPD in PBS led to a nearly complete (∼95%) fluorescence quenching compared with free BPD in DMSO (Fig. 2B). In contrast, nanoliposomes facilitated monomerization of photosensitizers. Up to 75% "recovery" of BPD's 690 nm peak was restored by the nanoliposomes (Fig. 2C). The BPD's fluorescence emission was restored by 40% in PBS (Fig. 2D).

We further tested whether L-BPD can be photoactivated to generate cytotoxic $^1O_2$ in serum-containing medium. Upon light-activation of L-BPD, we observed a light-dose–dependent decrease of BPD fluorescence due to photobleaching of BPD (Fig. 2E). Approximately 20% of BPD molecules in nanoliposomes were photobleached at 75 J/cm^2, and this was found similar to the photobleaching of free BPD molecules that are well dispersed in DMSO. Subsequently, the formation of $^1O_2$ upon light-activation of L-BPD was monitored using SOSG sensors. During light irradiation of L-BPD, we observed a dose-dependent increase of SOSG fluorescence intensity, which was markedly higher than that generated by free BPD under the same conditions (Fig. 2F). These data suggested that nanoliposomes retain a significant portion of BPD in their monomeric photoactive form. Therefore, L-BPD could effectively produce cytotoxic $^1O_2$ upon photoactivation.

Photodestruction of ABCG2 increases intracellular irinotecan

A major obstacle encountered in cancer chemotherapy is multidrug resistance, a process mediated by ATP-binding cassette (ABC) transmembrane transporters that utilize energy from ATP-binding/hydrolysis to actively pump chemotherapeutic agents out of cells (21). Overexpression of ABCG2 confers chemoresistance to pancreatic cancer cells and limits irinotecan efficacy (22). Several ABC transporter inhibitors have been investigated, but their drug–drug interactions with chemotherapeutic agents and toxicities limited their clinical usage (23). It is known that BPD is a substrate for ABCG2 (24), and others have suggested the possibility of photochemical destruction of "ABCG2-rich" extracellular vesicles (25). Here, we demonstrated that noncytotoxic low-dose PDT at 0.5 J/cm^2 (Supplementary Fig. S2A and S2B) significantly reduced the ABCG2 immunofluorescence signal from MIA PaCa-2 by approximately 70% at 1 and 6 hours post-PDT (Fig. 3A). Western blots confirmed decreased protein levels of ABCG2 at these time points in MIA PaCa-2 cells following the same PDT dose (Fig. 3B). Similar changes were observed in AsPC-1 cells (Supplementary Fig. S2C–S2E).

Given this PDT-based modulation of ABCG2, for which irinotecan is a known substrate, we subsequently tested whether PDT-mediated ABCG2 reduction could affect intracellular irinotecan accumulation. We observed that MIA PaCa-2 cells treated with combination of PDT and L-IRI showed 28% ± 7% and 49% ± 2%

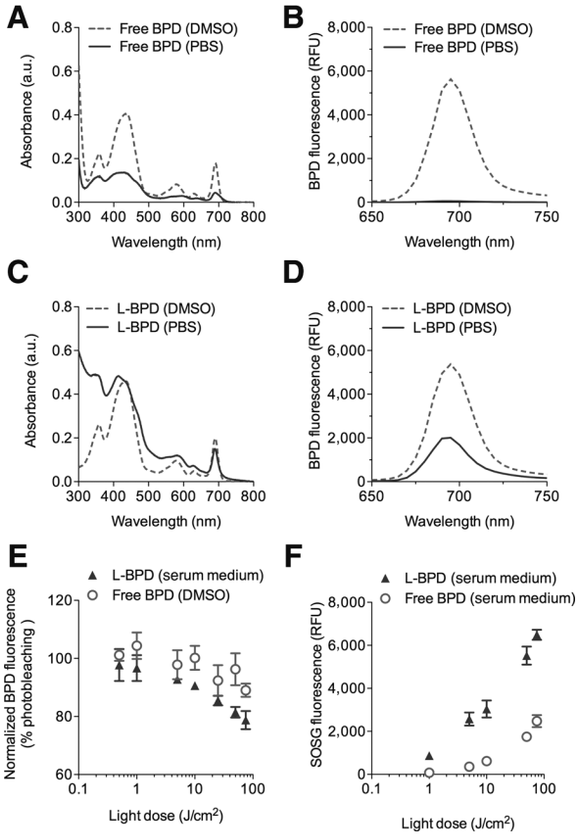

Figure 2.
L-BPD photophysical characterization. A, reduced absorbance intensity of free BPD in PBS (solid line) compared with free BPD in DMSO (dotted line), due to aggregation (self-quenching) of hydrophobic BPD in PBS. B, fluorescence of free BPD is quenched in PBS. C, formulating BPD in nanoliposomes as L-BPD restores absorbance of BPD in PBS (solid line). D, nanoliposomes dequench and recover BPD fluorescence in PBS. Values are in relative fluorescence units (RFU). E, BPD photobleaching post-PDT as a function of light dose (0.5–75 J/cm^2) determined by BPD fluorescence. F, SOSG reports $^1O_2$ production from photoactivated L-BPD and free BPD in medium ($N \geq 3$).

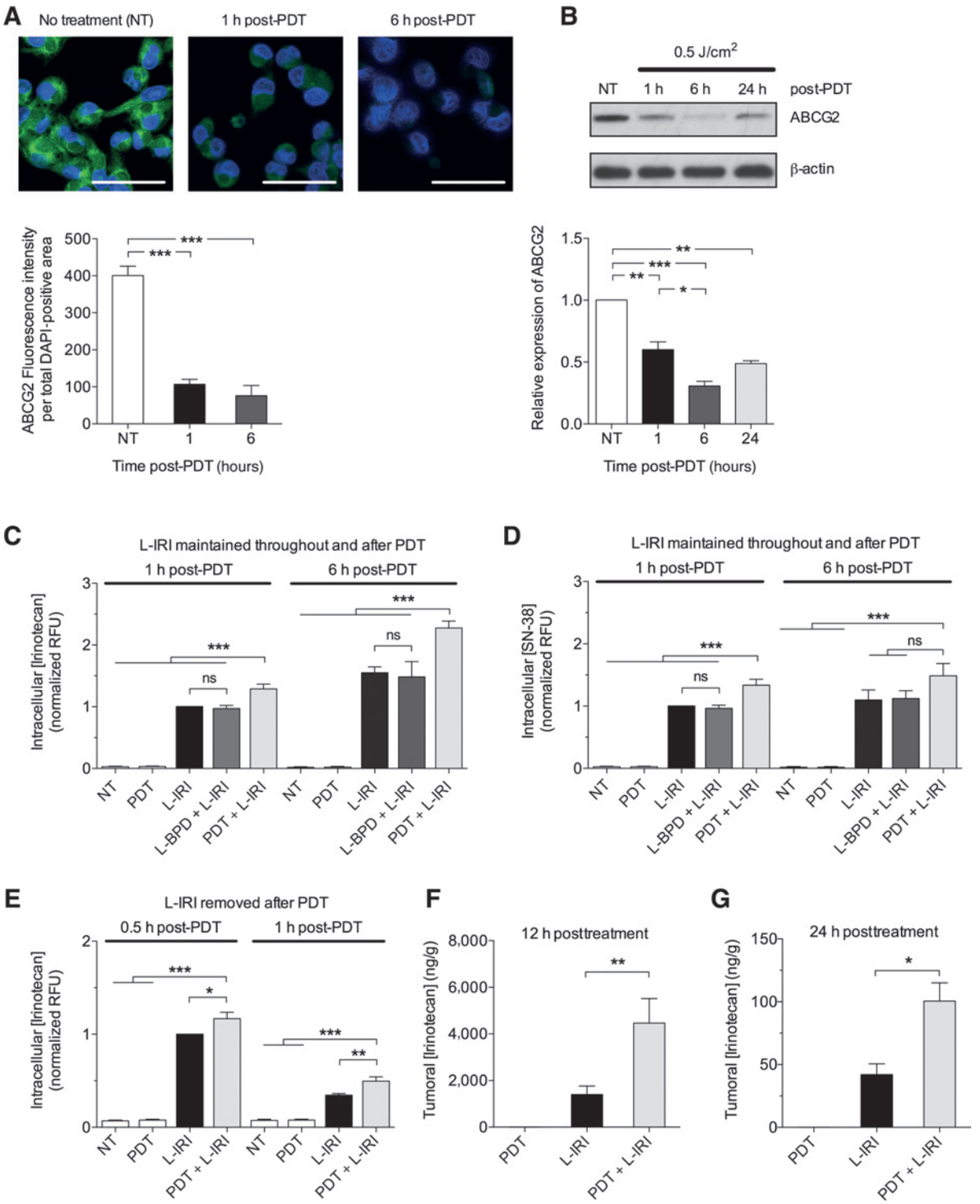

Figure 3.

Subcytotoxic PDT (L-BPD, 0.25 μmol/L; $h\nu$, 690 nm, 0.5 J/cm^2) reduces ABCG2 expression and increases intracellular irinotecan in MIA PaCa-2. A, immunofluorescence imaging of MIA PaCa-2 cells post-PDT. ABCG2 signal (green) is decreased at 1 and 6 hours post-PDT. Nuclei stained blue with DAPI. Scale bar, 50 μm. ABCG2 fluorescence intensity quantified per DAPI area. B, immunoblotting of ABCG2 in cell lysates collected 1, 6, and 24 hours post-PDT shows reduced ABCG2 expression. ABCG2 expressions relative to no-treatment were normalized to β-actin. C and D, intracellular levels of irinotecan and SN-38 increased post-PDT. MIA PaCa-2 cells were incubated with L-IRI (0.24 mg/mL) and L-BPD (0.25 μmol/L) for 1 hour before replacing with L-IRI–containing media (0.24 mg/mL) immediately before irradiation. Intracellular irinotecan levels from cell lysates at 1 and 6 hours post-PDT were determined by fluorescence signals of irinotecan (Ex/Em:355/460 nm) and SN-38 (Ex/Em:355/538 nm). E, following incubation with media containing L-IRI (0.24 mg/mL) and L-BPD (0.25 μmol/L) for 1 hour, fresh media (no L-IRI) was added immediately before irradiation such that any increase in irinotecan levels is only due to retention. Readouts in relative fluorescence units (RFU) were normalized to protein concentration. F and G, *in vivo*, irinotecan per gram of tumor (ng/g) increased at 12 and 24 hours post-PDT (*, $P < 0.05$; **, $P < 0.01$; ***, $P < 0.001$; one-way ANOVA Tukey range test; $N = 3$–6).

increases in intracellular irinotecan concentrations at 1 and 6 hours post-PDT, compared with cells treated with L-IRI alone (Fig. 3C). MIA PaCa-2 treated with both PDT and L-IRI also showed statistically significant enhancement in intracellular SN-38 (an active metabolite of irinotecan) over cells treated with L-IRI at 1-hour post-PDT. Increase in intracellular SN-38 was not significant at 6 hours post-PDT (Fig. 3D). This saturation of SN-38 is presumably due to a limited intracellular concentration of the carboxylesterase enzyme (26), which is responsible for conversion of irinotecan to SN-38. L-BPD alone (without light) did not increase intracellular concentrations of irinotecan and SN-38. In a separate study, L-IRI was removed from the media immediately before PDT, such that there is no contribution from uptake of L-IRI due to PDT. Higher intracellular levels of irinotecan were observed 1 hour post-PDT, suggesting that higher amounts of irinotecan were "retained" in cells (Fig. 3E). Similar enhancements of intracellular irinotecan and SN-38 concentrations post-PDT were observed in AsPC-1 (Supplementary Fig. S2F and S2G). These promising results prompted us to determine whether the combination would improve irinotecan accumulation *in vivo*. Indeed, the combination significantly ($P < 0.05$) increased intratumoral irinotecan levels by 3.2-fold and 2.4-fold at 12 and 24 hours post-PDT, respectively, as compared with L-IRI alone (Fig. 3F and G).

Irinotecan downregulates tumoral MCT-4 expression upregulated by PDT

Sections from MIA PaCa-2 tumors, excised 24 hours posttreatment, were stained with (i) CD31 (white) to identify vasculature; (ii) pimonidazole (green), a bioreductive chemical probe that forms protein adducts in viable hypoxic cells with partial oxygen pressure (pO_2) less than 10 mmHg in tumors; (iii) MCT-4 (red), a lactate efflux pump that allows cancer cells to utilize aberrant glycolytic metabolism and can be influenced by abnormal tumor microenvironment such as that caused by hypoxia (27); and, (iv) DAPI (blue) to mark nuclei. Figure 4 shows representative immunofluorescence images for these biomarkers in MIA PaCa-2 tumors at 24 hours posttreatment, as well as the corresponding quantification of MCT-4 expression, a biomarker that has been linked with poor prognosis in pancreatic cancer (28). In determining the treatment-induced changes in MCT-4 expression, we separately analyzed pimonidazole positive and pimonidazole negative regions, as pimonidazole only stains distinct regions with pO_2 below 10 mmHg. These areas are typically adjacent to necrotic zones that are chronically and severely depleted of oxygen and, thus, could potentially exhibit a differential response profile from other regions. The MCT-4 intensity was normalized to DAPI intensity in either pimonidazole negative regions only (Fig. 4A and C) or the whole cross-tumor section irrespective of pimonidazole status (Fig. 4D).

We demonstrated *in vivo* that L-IRI reduced the immunofluorescence signal of MCT-4 by approximately 52% at 24 hours postinjection compared with no-treatment controls in pimonidazole-negative regions, while PDT increased MCT-4 staining compared with no-treatment (Fig. 4A and C). In the combination group, MCT-4 significantly decreased ($P < 0.001$) in non-pimonidazole–stained areas compared with no-treatment controls. Similarly, when both pimonidazole-positive and -negative regions were considered, a decrease ($P < 0.05$) in MCT-4 signal was also observed in L-IRI and combination groups (Fig. 4B and D). However, this magnitude of difference is less pronounced, suggesting that MCT-4 expression may be harder to affect in regions with low pO_2 ($\leq$10 mmHg). Overall, these results indicate that in combination, L-IRI acts to reduce the expression of MCT-4, which we observe to be upregulated by oxygen-consuming BPD-PDT.

Survivin-downregulating PDT in combination with L-IRI enhances apoptosis *in vivo*

Survivin, an inhibitor of apoptosis, plays an essential role in regulating apoptosis by inhibiting caspases (29). Decreased survivin expression has been shown to enhance the efficacy of camptothecin analogues for several cancers (30). Gomer and colleagues and others demonstrated that PDT can regulate survivin expression in cancers, and such apoptotic modulation is dependent on photosensitizer and cell type (31). At 24 hours post-PDT, we observe that PDT decreased survivin expression in MIA PaCa-2 and AsPC-1 cells, both *in vivo* and *in vitro* (Fig. 5A–C). In addition, immunoblots of MIA PaCa-2 tumors show that survivin expression remained low *in vivo* at 24 hours after the combination treatment (Fig. 5C). In these same tumors, we observe a concomitant increase in tumoral expression of cleaved caspase-3 and cleaved PARP overall. Together, the low expression of survivin and increased levels of cleaved PARP and cleaved caspase-3 suggest that the combination enhances apoptosis *in vivo*, relative to the monotherapies.

Combination treatment enhances tumor growth inhibition

The above mechanistic insights provided us a compelling rationale to assess the combination of PDT and L-IRI in orthotopic mouse models of MIA PaCa-2 and AsPC-1. Metastasis-derived AsPC-1 tumors exhibited faster growth rates than MIA PaCa-2 (Supplementary Fig. S3), in accordance with previous reports citing differences in tumorigenicity, immunocytochemistry, and histology for these cell lines (32). A single low-dose combination of PDT (L-BPD: 0.25 mg/kg) and L-IRI (20 mg/kg) demonstrated superior MIA PaCa-2 tumor volume growth inhibition by approximately 70% for at least 3 weeks, compared with <25% reduction after monotherapies (Fig. 6A). The slope of linearized growth curves for the combination group (PDT+L-IRI) was significantly lower ($P = 0.0191$) than the "sum" of the slopes for both monotherapies (PDT alone and L-IRI alone), suggesting the combination is synergistic (Supplementary Table S3).

At 3 weeks posttreatment (30 days postimplantation), tumor weights in the combination group (195 $\pm$ 30 mg) were significantly lower ($P < 0.05$) than that of no-treatment (373 $\pm$ 45 mg) and L-BPD groups (399 $\pm$ 30 mg; Fig. 6B). There was no statistically significant difference in tumor weight between the L-IRI (314 $\pm$ 24 mg) and L-BPD+L-IRI groups (318 $\pm$ 57 mg), suggesting that L-BPD alone without light is not tumoricidal. Although tumor weights in the combination group (195 $\pm$ 30 mg) were lower than that in the L-IRI group (314 $\pm$ 24 mg), this was not statistically significant. Given this observation, we also compared changes in tumor volume at 2 weeks posttreatment (i.e., right before tumor regrowth was observed in the combination group; Fig. 6C). Interestingly, at 2 weeks posttreatment, the fold-increase in tumor volume for the combination group ($\sim$1.8-fold) was found to be significantly lower than the L-IRI group ($\sim$5.2-fold), L-BPD+L-IRI group ($\sim$5.1-fold), and no-treatment

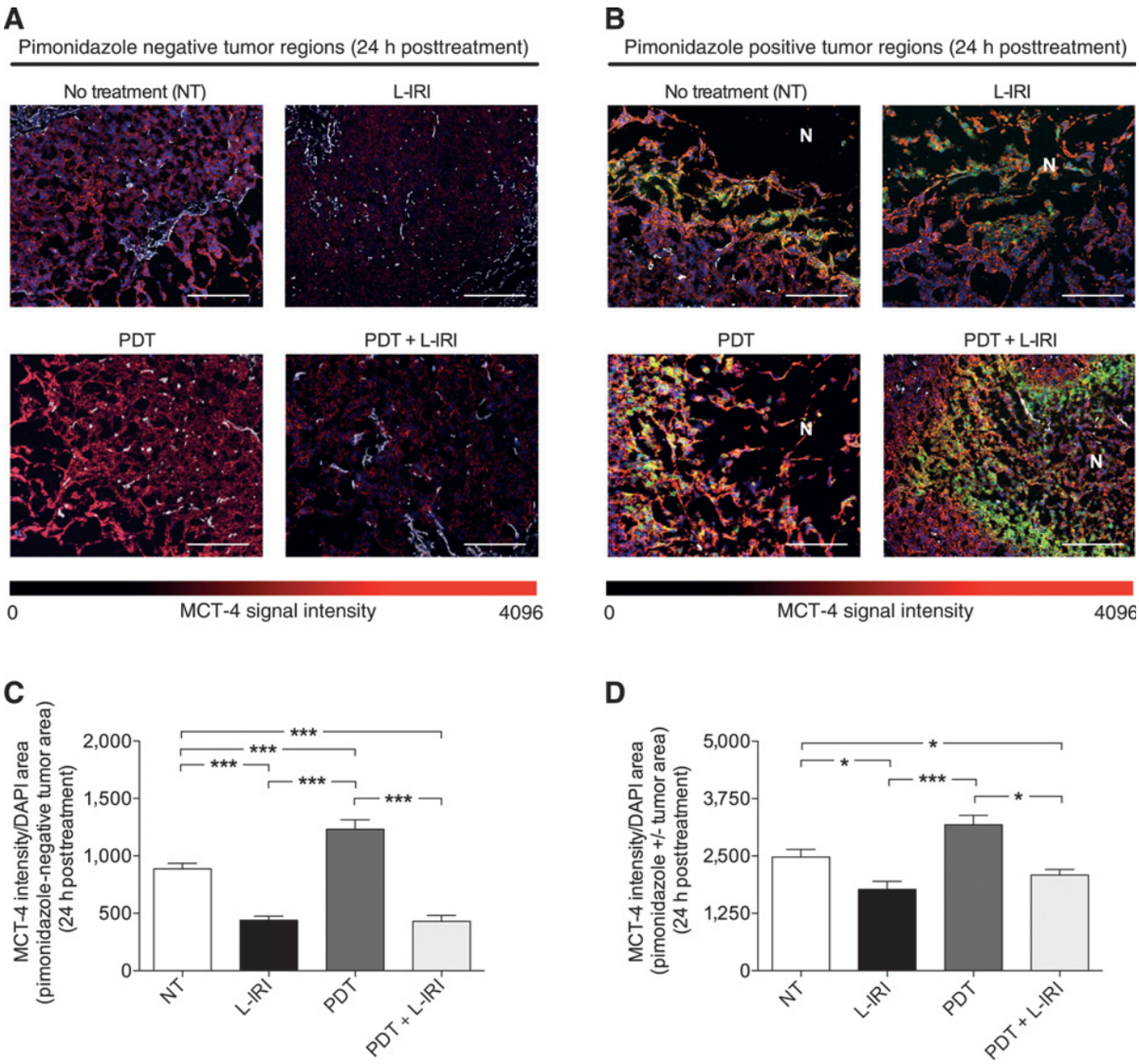

Figure 4.

L-IRI reduces MCT-4 expression, which is upregulated by PDT. A and B, immunofluorescence images of regions with and without pimonidazole (green), respectively, in MIA PaCa-2 tumors 24 hours posttreatment showing CD31 for endothelial cells (white) and MCT-4 (red). Scale bar, 500 μm. N, necrosis. C, MCT-4 (red) intensity increases with oxygen-consuming PDT, but reduces with L-IRI in both L-IRI alone and combination groups. D, similar changes in MCT-4 expression observed in both pimonidazole-positive and -negative regions (*, $P < 0.05$; ***, $P < 0.001$; one-way ANOVA Tukey range test; $N \geq 15$).

group (~5.9-fold), but not significantly different than the PDT group (~3.3-fold). These data suggest that this combination balances the initial PDT actions with the sustained irinotecan therapeutic effects. *In vivo* efficacy of the combination regimen was further evaluated in AsPC-1 tumors. At 3 weeks posttreatment, a single combination treatment cycle reduced AsPC-1 tumor volume (Fig. 6D) and weight (Fig. 6E) by an average of 66.6% and 58.1%, respectively, compared with no-treatment. In contrary, tumor weights and volumes in the PDT (e.g., 260 ± 86 mm^2) and L-IRI groups (e.g., 219 ± 28 mm^2) were not significantly different from no-treatment (e.g., 302 ± 48 mm^2).

For both MIA PaCa-2 and AsPC-1, tumor regrowth was observed 10 to 14 days after a single cycle of low-dose combination treatment. A second cycle of low-dose combination therapy prolonged the inhibition of MIA PaCa-2 tumor growth up to 42 days postimplantation (Fig. 6F). No animal death or changes in mouse weight were observed (Supplementary Fig. S4). General behavior and physiologic activities of mice were normal as per IACUC guidelines.

Effect of PDT and L-IRI on tumor-related biomarkers

Studies show that MVD estimation is a promising treatment response indicator (33). Here, we evaluate MVD via CD31-staining of vascular endothelial cells to determine tumor vascularization. Confocal images of MIA PaCa-2 cross-sections at 3-weeks posttreatment show immunostaining of both endothelial cells (green) and Ki-67 (proliferation marker, red) are significantly

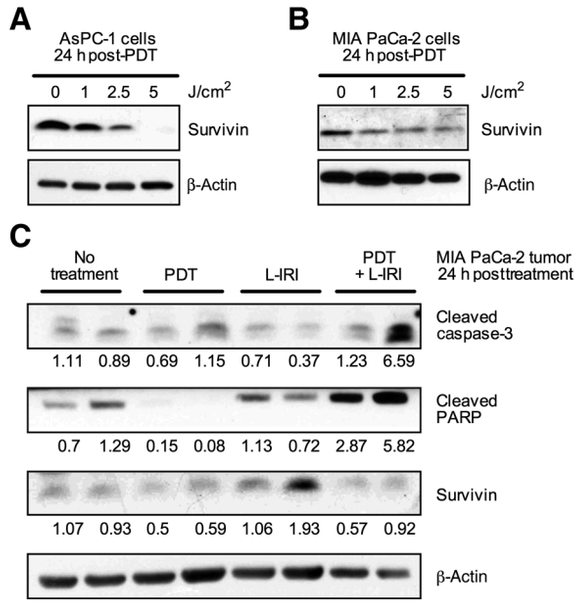

Figure 5.
PDT decreases survivin *in vitro* and *in vivo*. A and B, AsPC-1 and MIA PaCa-2 cells collected 24 hours post-PDT (L-BPD: 0.25 μmol/L) show dose-dependent decrease in survivin by immunoblotting. C, tissue lysates from two individual MIA PaCa-2 tumors collected 24 hours post-PDT suggest that survivin expression is not upregulated in the combination treatment. Corresponding increases in proapoptotic markers, cleaved caspase-3, and cleaved PARP are observed. Densitometry values are normalized to β-actin.

lower in the combination group compared with no-treatment (Fig. 7A). White arrows indicate microvessels, which are clearly smaller post-combination therapy. Quantitative analyses revealed that the combination resulted in a significant decrease ($P < 0.05$) in MVD by approximately 30%, whereas suboptimal PDT alone or L-IRI alone did not reduce tumoral MVD (Fig. 7C). Consistent with this antivascular effect, quantitative analyses revealed a dramatic ($P < 0.05$) reduction of Ki-67-staining by >60% in tumors receiving the combination treatment, compared with no-treatment (Fig. 7D). Supporting the synergistic impact of the treatments on proliferation and vasculature destruction, we observed enhanced necrotic volumes in combination-treated tumors compared with all other groups (Fig. 7B and E). A low-dose combination treatment provided sustained tumor growth inhibition but did not eradicate the tumor completely. Indeed, H&E images of tumors in combination treatment group (Fig. 7B) show a viable rim of tumor 3 weeks posttreatment, indicating the necessity of multiple treatments for potentially complete treatment.

Discussion

The uniqueness of the PDT and L-IRI combination is that they mechanistically cooperate with each other, beyond their individual tumor destruction pathways, to enhance reduction in tumor burden with nonoverlapping toxicities. Here, three cooperative pathways are demonstrated to elucidate the synergism: (i) PDT reduces ABCG2 expression, thereby increasing intracellular irinotecan and SN-38 levels; (ii) irinotecan reduces tumoral expression of MCT-4, which is upregulated by PDT; (iii) PDT downregulates survivin expression, and amplification of the apoptotic and antiproliferative effects was observed in the combination. The dramatic enhancement in tumor growth inhibition by the combination treatment confirms the strength of developing mechanistically cooperative combinations, where each monotherapy enhances and benefits from the other, for difficult-to-treat diseases, such as pancreatic cancer.

Late diagnosis and limited effectiveness of standard treatments have resulted in a 5-year survival rate of $\leq$5% in pancreatic cancer patients (34). Pancreatic cancer is notoriously resistant to chemoradiotherapies, partly attributable to inherent genetic complexities and abnormal microenvironment (35). Several combination therapies have been clinically evaluated for pancreatic cancer, but most were abandoned due to ineffectiveness and high toxicities (36). Recently, Abraxane plus gemcitabine showed modest 2-month improvements in median OS compared with gemcitabine alone (37). FOLFIRINOX, a combination of four chemotherapeutic agents (leucovorin, fluorouracil, irinotecan, oxaliplatin), generated much excitement after extending the median OS from 6.8 to 11.1 months (38). However, FOLFIRINOX is limited to a small proportion of healthy patients due to high toxicities. Against this background, PDT is emerging as a clinically promising locoregional therapy for pancreatic cancer (13, 14), given its efficacy against gemcitabine-insensitive cells (39), synergism with chemo/biologic agents, and low incidence of mild adverse events clinically (14). PDT has also been shown to induce antitumor immunity in various immunocompetent cancer models (40).

Driven by this concept of developing rapidly translatable combinations where each component reinforces the other, our study is motivated by advances in nanoliposomal BPD-based PDT (phase I/II) and the recently FDA-approved nanoliposomal irinotecan (Onivyde) for pancreatic cancer (4, 14, 41). In this study, nanoliposomes improved the photochemical stability of BPD and the circulation profile of irinotecan, supporting the reduced systemic toxicity, and increased efficacy of nanoliposomal BPD and irinotecan that have been established (20, 42). In our *in vivo* combination, L-BPD and L-IRI were administered intravenously simultaneously and PDT was performed 1 hour postinjection, when both agents were readily available at the tumor for their cooperative therapeutic actions.

Here, sublethal PDT reduced ABCG2 expression and increased intracellular concentrations of irinotecan and SN-38 by up to approximately 50% 6 hours posttreatment (Fig. 3C and D), whereas L-BPD alone does not interfere with intracellular irinotecan accumulation. Moreover, PDT-mediated ABCG2 reduction was sustainable for up to 24 hours (Fig. 3B). Studies have shown that durable maintenance of high intratumoral irinotecan and SN-38 levels is a critical determinant of antitumor activity (43). Therefore, a sustained window of ABCG2-reduction could be important for enhanced irinotecan efficacy. It should be noted that at 24 hours, expression of ABCG2 appears to recover (Fig. 3B), although remaining lower than pre-PDT levels. This observation suggests that subsequent treatments of PDT and future optimization of PDT dose may be warranted for prolonged ABCG2 reduction.

In vivo, PDT (one-hour L-BPD-light interval) enhanced intratumoral irinotecan accumulation by more than 3-fold at 12 hours posttreatment, compared with L-IRI alone. Our previous work demonstrated that PDT with 1-hour BPD-light interval targets both tumor cells and vasculature (44). Therefore, it is important to

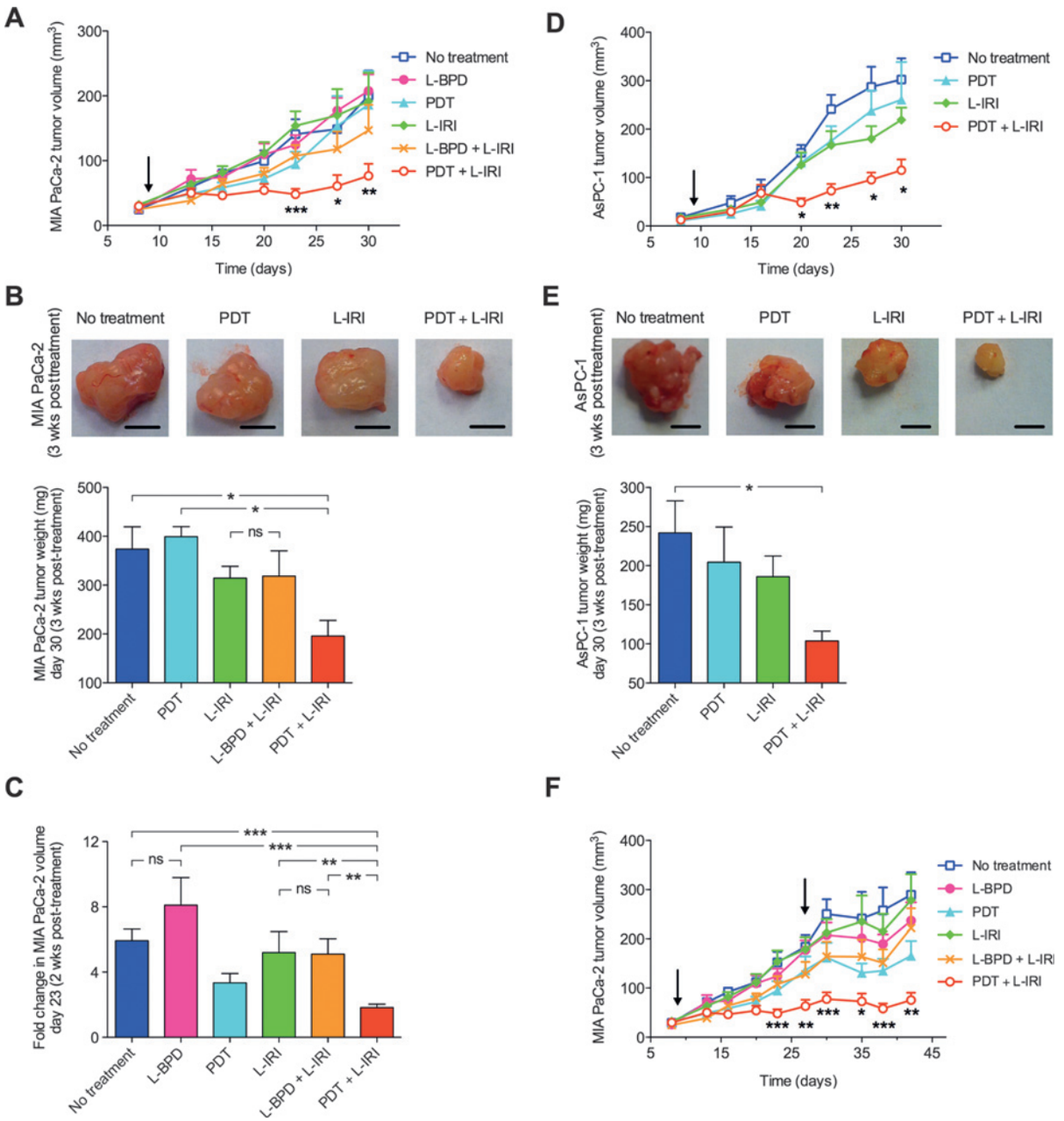

Figure 6.
Combination therapy inhibits tumor growth. A, combination PDT and L-IRI enhanced MIA PaCa-2 tumor volume reduction, determined by longitudinal ultrasound imaging. B, representative snapshots of MIA PaCa-2 tumors 3 weeks posttreatment. Scale bar, 2 cm. Tumor weights at this time showed the combination inhibited tumor growth. C, fold change in tumor volume 2 weeks posttreatment shows significantly lower volume in the combination group. D, combination PDT and L-IRI also enhanced AsPC-1 tumor volume reduction. E, representative snapshots of AsPC-1 tumors 3 weeks posttreatment. Scale bar, 2 cm. Tumor weights at this time showed the combination slowed tumor growth. F, a sustained and prolonged MIA PaCa-2 tumor growth inhibition was observed after two cycles of combination administered on 9 and 27 days postimplantation. Arrow, day of treatment (*, $P < 0.05$; **, $P < 0.01$; ***, $P < 0.001$, Kruskal–Wallis one-way ANOVA; $N = 8$–18).

note that, besides the reduction of cellular ABCG2 expression, other mechanisms could also contribute to PDT-mediated enhancement of intratumoral drug accumulation. Previous studies have shown that BPD-PDT at a short photosensitizer-light interval of 15 minutes mainly causes vascular permeabilization, which leads to a modest enhancement (≤2-fold) of macromolecule delivery to tumors (45). Future studies varying the photosensitizer-light interval to balance cellular damage (including ABCG2 photodestruction) and vascular permeabilization for maximal drug accumulation are merited. Although many attempts have been made to enhance the chemotherapy effectiveness by overcoming ABC transporter-mediated drug efflux

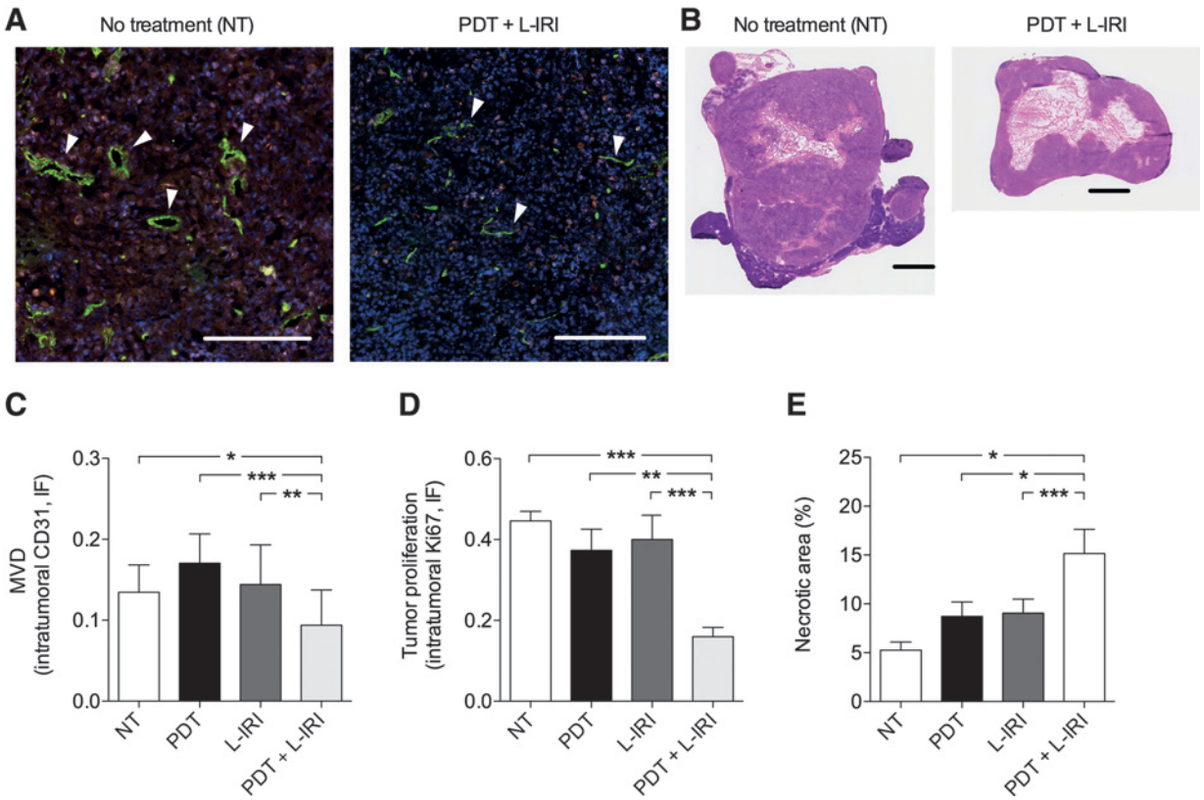

Figure 7.
Antivascular and antiproliferation effects 3 weeks posttreatment (30 days postimplantation). A, representative fluorescence images of MIA PaCa-2 tumor cross-section with immunostaining of endothelial cells (green), Ki-67 (red), and nuclei (blue) without and with combination therapy. Arrows, microvessels. Scale bar, 250 μm. B, hematoxylin (H&E) images of MIA PaCa-2 cross-sections 3 weeks posttreatment. Scale bar, 1 cm. C–E, quantitative analyses revealed that a single combination decreased intratumoral MVD as determined by CD31 intensity, inhibited pancreatic cancer proliferation as determined by Ki-67 and enhanced necrosis (*, $P < 0.05$; **, $P < 0.01$; ***, $P < 0.001$; one-way ANOVA Tukey range test; $N \geq 11$ cross-sections from $N \geq 3$ mice/group).

with small-molecule inhibitors, most studies have failed due to drug interactions and systemic toxicities (23). PDT, an FDA-approved regimen with nonoverlapping toxicities, provides a unique opportunity for inhibition of irinotecan efflux transporters, while avoiding those toxicity-related pitfalls.

Several studies have shown that oncogenic Ras-driven signals in pancreatic cancer cells can propel abnormal metabolic alterations, such as dependence on glycolysis. MCT-4 is a critical component in the glycolytic metabolism of pancreatic cancer cells, and can be further upregulated via several tumor microenvironmental changes such as hypoxia (27). Studies have shown that high MCT-4 expression is a poor prognostic indicator in pancreatic cancer and that inhibition of MCT-4 leads to tumor growth suppression and increased cellular apoptosis (28). PDT can create tumor hypoxia when oxygen is depleted by photochemical consumption or when oxygen supply is compromised by microvascular damage (46). These hypoxic conditions can stimulate metabolic alterations, harbor treatment resistant cells, and drive the cells towards metastatic invasion through activation of pathways, such as HIF1α (47). A unique feature of our combination is that irinotecan alleviates a compensatory response elicited by PDT. We show that although PDT elevates MCT-4 expression, the irinotecan component of the combination mitigates this increase and reduces MCT-4 to levels comparable with irinotecan treatment alone (Fig. 4). This observed effect, in accordance with the ability of irinotecan to downregulate HIF1α as reported by others (48), may also reduce metastatic dissemination of the disease in the combination treatment, and is currently being investigated. A sustained decrease in MVD is observed with the combination treatment compared with other groups at 3-weeks posttreatment (Fig. 7). Although chronic vascular damage likely contributes to enhanced growth arrest, nutrient depletion and reduced blood supply could potentially lead to further hypoxia and corresponding survival signals. These conditions suggest that multiple irinotecan cycles may further enhance the two therapies' synergism, through its effect on hypoxia-induced markers. Although reduction of blood supply may have been a concern for delivery of subsequent treatments, a second dose of the combination at 27 days postimplantation continues to exhibit synergistic efficacy and prolongs significant tumor growth inhibition (Fig. 6F).

Reduction in systemic toxicity is another attractive feature of PDT and L-IRI combination. Clinically, irinotecan can be prescribed for up to 12 cycles. However, due to its significant systemic toxicities (grade 3–4 diarrhea and neutropenia), patients receive an average of six cycles and often require dose reductions, compromising the chemo-effectiveness. PDT is associated with low incidence of mild abdominal pain, which can be relieved with analgesia. Normal pancreatic tissue healing has been shown after interstitial PDT without significant impact to structure or function (14). In addition to nonoverlapping side effects, the combination

of PDT and L-IRI is significant in that enhanced cytotoxic efficacy can be achieved using drug doses at 12- to 20-fold lower than equivalent clinical doses (Supplementary Table S1). In this study, we demonstrated that a single cycle, low-dose combination dramatically inhibited tumor volume growth by 70%, while others demonstrated that five doses of standard gemcitabine (250 mg/kg) is ineffective against orthotopic MIA PaCa-2 tumors (49). A second cycle of combination therapy further prolonged MIA PaCa-2 tumor growth inhibition, and was well tolerated by mice. This compares favorably with the modest (~30%) tumor weight reduction of orthotopic pancreatic cancer tumors after six cycles of 25 mg/kg irinotecan (50).

In summary, this study shows that low-dose combination of PDT and L-IRI synergistically enhanced tumor growth inhibition compared with either treatment alone and was more effective than reported outcomes with a standard chemotherapeutics for pancreatic cancer (49, 50). Given the clinical promise of the individual therapies, this combination is easily translatable for clinical management of pancreatic cancer and other cancers. Further studies using multicycle dosing for durable response, and evaluating metastasis control and survival enhancement are merited.

Disclosure of Potential Conflicts of Interest

No potential conflicts of interest were disclosed.

Authors' Contributions

Conception and design: H.-C. Huang, S. Mallidi, J. Liu, C.-T. Chiang, I. Rizvi, T. Hasan

Development of methodology: H.-C. Huang, S. Mallidi, C.-T. Chiang, I. Rizvi, T. Hasan

Acquisition of data (provided animals, acquired and managed patients, provided facilities, etc.): H.-C. Huang, S. Mallidi, J. Liu, C.-T. Chiang, Z. Mai, R. Goldschmidt

Analysis and interpretation of data (e.g., statistical analysis, biostatistics, computational analysis): H.-C. Huang, S. Mallidi, J. Liu, C.-T. Chiang, N. Ebrahim-Zadeh, I. Rizvi

Writing, review, and/or revision of the manuscript: H.-C. Huang, S. Mallidi, J. Liu, C.-T. Chiang, N. Ebrahim-Zadeh, I. Rizvi, T. Hasan

Administrative, technical, or material support (i.e., reporting or organizing data, constructing databases): H.-C. Huang, S. Mallidi

Study supervision: H.-C. Huang, S. Mallidi, T. Hasan

Acknowledgments

The authors thank Dr. Zhao and Mrs. Wu (WCP Photopathology) for help with histology, Dr. Schoenfeld (MGH Biostatistics Center) for support in statistical analyses, and Drs. Spring and Palanisami for discussions.

Grant Support

This work was supported by NIH grants P01CA084203, R01CA156177, R01CA160998, S10ODO1232601 (T. Hasan), MGH-Tosteson-FMD-Fellowship 224889 (H.C. Huang), F32CA165881 (S. Mallidi), and K99CA175292 (I. Rizvi)

The costs of publication of this article were defrayed in part by the payment of page charges. This article must therefore be hereby marked *advertisement* in accordance with 18 U.S.C. Section 1734 solely to indicate this fact.

Received February 7, 2015; revised November 10, 2015; accepted December 10, 2015; published OnlineFirst December 30, 2015.

References

1. Hanahan D, Weinberg Robert A. Hallmarks of cancer: the next generation. Cell 2011;144:646–74.
2. Al-Lazikani B, Banerji U, Workman P. Combinatorial drug therapy for cancer in the post-genomic era. Natre Biotechnol 2012;30:679–92.
3. Pommier Y, Leo E, Zhang H, Marchand C. DNA topoisomerases and their poisoning by anticancer and antibacterial drugs. Chem Biol 2010;17:421–33.
4. Ko AH, Tempero MA, Shan YS, Su WC, Lin YL, Dito E, et al. A multinational phase 2 study of nanoliposomal irinotecan sucrosofate (PEP02, MM-398) for patients with gemcitabine-refractory metastatic pancreatic cancer. Br J Cancer 2013;109:920–5.
5. Saif MW. MM-398 achieves primary endpoint of overall survival in phase III study in patients with gemcitabine refractory metastatic pancreatic cancer. JOP 2014;15:278–9.
6. Celli JP, Spring BQ, Rizvi I, Evans CL, Samkoe KS, Verma S, et al. Imaging and photodynamic therapy: mechanisms, monitoring, and optimization. Chem Rev 2010;110:2795–838.
7. Kessel D, Castelli M. Evidence that bcl-2 is the target of three photosensitizers that induce a rapid apoptotic response. Photochem Photobiol 2001;74:318–22.
8. Xue LY, Chiu SM, Oleinick NL. Photochemical destruction of the Bcl-2 oncoprotein during photodynamic therapy with the phthalocyanine photosensitizer Pc 4. Oncogene 2001;20:3420–7.
9. Spring BQ, Rizvi I, Xu N, Hasan T. The role of photodynamic therapy in overcoming cancer drug resistance. Photochem Photobiol Sci 2015;14:1476–91.
10. Duska LR, Hamblin MR, Miller JL, Hasan T. Combination photoimmunotherapy and cisplatin: effects on human ovarian cancer ex vivo. J Natl Cancer Inst 1999;91:1557–63.
11. Gallagher-Colombo SM, Miller J, Cengel KA, Putt ME, Vinogradov SA, Busch TM. Erlotinib pretreatment improves photodynamic therapy of non-small cell lung carcinoma xenografts via multiple mechanisms. Cancer Res 2015;75:3118–26.
12. del Carmen MG, Rizvi I, Chang Y, Moor AC, Oliva E, Sherwood M, et al. Synergism of epidermal growth factor receptor-targeted immunotherapy with photodynamic treatment of ovarian cancer *in vivo*. J Natl Cancer Inst 2005;97:1516–24.
13. Bown SG, Rogowska AZ, Whitelaw DE, Lees WR, Lovat LB, Ripley P, et al. Photodynamic therapy for cancer of the pancreas. Gut 2002;50:549–57.
14. Huggett MT, Jermyn M, Gillams A, Illing R, Mosse S, Novelli M, et al. Phase I/II study of verteporfin photodynamic therapy in locally advanced pancreatic cancer. Br J Cancer 2014;110:1698–704.
15. Torchilin VP. Recent advances with liposomes as pharmaceutical carriers. Nat Rev Drug Discov 2005;4:145–60.
16. Chowdhary RK, Shariff I, Dolphin D. Drug release characteristics of lipid based benzoporphyrin derivative. J Pharm Pharm Sci 2003;6:13–9.
17. Akbarzadeh A, Rezaei-Sadabady R, Davaran S, Joo SW, Zarghami N, Hanifehpour Y, et al. Liposome: classification, preparation, and applications. Nanoscale Res Lett 2013;8:102.
18. Szoka F Jr, Papahadjopoulos D. Procedure for preparation of liposomes with large internal aqueous space and high capture by reverse-phase evaporation. Proc Natl Acad Sci U S A 1978;75:4194–8.
19. Kaneda N, Nagata H, Furuta T, Yokokura T. Metabolism and pharmacokinetics of the camptothecin analogue CPT-11 in the mouse. Cancer Res 1990;50:1715–20.
20. Chen B, Pogue BW, Hasan T. Liposomal delivery of photosensitising agents. Expert Opin Drug Deliv 2005;2:477–87.
21. Rees DC, Johnson E, Lewinson O. ABC transporters: the power to change. Nat Rev Mol Cell Biol 2009;10:218–27.
22. Konig J, Hartel M, Nies AT, Martignoni ME, Guo J, Buchler MW, et al. Expression and localization of human multidrug resistance protein (ABCC) family members in pancreatic carcinoma. Int J Cancer 2005;115:359–67.
23. Szakacs G, Paterson JK, Ludwig JA, Booth-Genthe C, Gottesman MM. Targeting multidrug resistance in cancer. Nat Rev Drug Discov 2006;5:219–34.
24. Liu W, Baer MR, Bowman MJ, Pera P, Zheng X, Morgan J, et al. The tyrosine kinase inhibitor imatinib mesylate enhances the efficacy of photodynamic therapy by inhibiting ABCG2. Clin Cancer Res 2007;13:2463–70.

25. Goler-Baron V, Assaraf YG. Overcoming multidrug resistance via photodestruction of ABCG2-rich extracellular vesicles sequestering photosensitive chemotherapeutics. PLoS ONE 2012;7:e35487.
26. Tobin P, Clarke S, Seale JP, Lee S, Solomon M, Aulds S, et al. The *in vitro* metabolism of irinotecan (CPT-11) by carboxylesterase and beta-glucuronidase in human colorectal tumours. Br J Clin Pharmacol 2006;62:122–9.
27. Ullah MS, Davies AJ, Halestrap AP. The plasma membrane lactate transporter MCT4, but not MCT1, is up-regulated by hypoxia through a HIF-1alpha-dependent mechanism. J Biol Chem 2006;281:9030–37.
28. Baek G, Tse YF, Hu Z, Cox D, Buboltz N, McCue P, et al. MCT4 defines a glycolytic subtype of pancreatic cancer with poor prognosis and unique metabolic dependencies. Cell Rep 2014;9:2233–49.
29. Li F, Ackermann EJ, Bennett CF, Rothermel AL, Plescia J, Tognin S, et al. Pleiotropic cell-division defects and apoptosis induced by interference with survivin function. Nat Cell Biol 1999;1:461–6.
30. Bevins RL, Zimmer SG. It's about time: scheduling alters effect of histone deacetylase inhibitors on camptothecin-treated cells. Cancer Res 2005;65:6957–66.
31. Ferrario A, Rucker N, Wong S, Luna M, Gomer CJ. Survivin, a member of the inhibitor of apoptosis family, is induced by photodynamic therapy and is a target for improving treatment response. Cancer Res 2007;67:4989–95.
32. Deer EL, Gonzalez-Hernandez J, Coursen JD, Shea JE, Ngatia J, Scaife CL, et al. Phenotype and genotype of pancreatic cancer cell lines. Pancreas 2010;39:425–35.
33. Jain RK, Duda DG, Willett CG, Sahani DV, Zhu AX, Loeffler JS, et al. Biomarkers of response and resistance to antiangiogenic therapy. Nat Rev Clin Oncol 2009;6:327–38.
34. Chrystoja CC, Diamandis EP, Brand R, Ruckert F, Haun R, Molina R. Pancreatic cancer. Clin Chem 2013;59:41–6.
35. Ghaneh P, Costello E, Neoptolemos JP. Biology and management of pancreatic cancer. Gut 2007;56:1134–52.
36. Gunturu KS, Rossi GR, Saif MW. Immunotherapy updates in pancreatic cancer: are we there yet? Ther Adv Med Oncol 2013;5:81–9.
37. Von Hoff DD, Ervin T, Arena FP, Chiorean EG, Infante J, Moore M, et al. Increased survival in pancreatic cancer with nab-paclitaxel plus gemcitabine. N Engl J Med 2013;369:1691–703.
38. Conroy T, Desseigne F, Ychou M, Bouche O, Guimbaud R, Becouarn Y, et al. FOLFIRINOX versus gemcitabine for metastatic pancreatic cancer. N Engl J Med 2011;364:1817–25.
39. Celli JP, Solban N, Liang A, Pereira SP, Hasan T. Verteporfin-based photodynamic therapy overcomes gemcitabine insensitivity in a panel of pancreatic cancer cell lines. Lasers Surg Med 2011;43:565–74.
40. Castano AP, Mroz P, Hamblin MR. Photodynamic therapy and anti-tumour immunity. Nat Rev Cancer 2006;6:535–45.
41. Wang-Gillam A, Li CP, Bodoky G, Dean A, Shan YS, Jameson G, et al. Nanoliposomal irinotecan with fluorouracil and folinic acid in metastatic pancreatic cancer after previous gemcitabine-based therapy (NAPOLI-1): a global, randomised, open-label, phase 3 trial. Lancet 2015. doi: 10.1016/S0140-6736(15)00986-1. [Epub ahead of print].
42. Drummond DC, Noble CO, Guo Z, Hong K, Park JW, Kirpotin DB. Development of a highly active nanoliposomal irinotecan using a novel intraliposomal stabilization strategy. Cancer Res 2006;66:3271–7.
43. Kalra AV, Kim J, Klinz SG, Paz N, Cain J, Drummond DC, et al. Preclinical activity of nanoliposomal irinotecan is governed by tumor deposition and intratumor prodrug conversion. Cancer Res 2014;74:7003–13.
44. Chen B, Pogue BW, Hoopes PJ, Hasan T. Combining vascular and cellular targeting regimens enhances the efficacy of photodynamic therapy. Int J Radiat Oncol Biol Phys 2005;61:1216–26.
45. Chen B, Pogue BW, Luna JM, Hardman RL, Hoopes PJ, Hasan T. Tumor vascular permeabilization by vascular-targeting photosensitization: effects, mechanism, and therapeutic implications. Clin Cancer Res 2006;12(3 Pt 1):917–23.
46. Henderson BW, Fingar VH. Relationship of tumor hypoxia and response to photodynamic treatment in an experimental mouse tumor. Cancer Res 1987;47:3110–4.
47. Wilson WR, Hay MP. Targeting hypoxia in cancer therapy. Nat Rev Cancer 2011;11:393–410.
48. Guerin E, Raffelsberger W, Pencreach E, Maier A, Neuville A, Schneider A, et al. *In vivo* topoisomerase I inhibition attenuates the expression of hypoxia-inducible factor 1α target genes and decreases tumor angiogenesis. Mol Med 2012;18:83–94.
49. Bornmann C, Graeser R, Esser N, Ziroli V, Jantscheff P, Keck T, et al. A new liposomal formulation of Gemcitabine is active in an orthotopic mouse model of pancreatic cancer accessible to bioluminescence imaging. Cancer Chemother Pharmacol 2008;61:395–405.
50. Li L, Yue GG, Fung KP, Leung PC, Lau CB, Leung PS. Establishment of an orthotopic model of pancreatic cancer to evaluate the antitumor effects of irinotecan through the biomarker carbohydrate antigen 19-9 in mice. Pancreas 2014;43:1126–8.